Optics Letters

Intensity surge and negative polarization of light from compact irregular particles

Yevgen Grynko,[1,*] Yuriy Shkuratov,[2] and Jens Förstner[1]

[1]Department of Theoretical Electrical Engineering, Paderborn University, Warburger Str. 100, 33102 Paderborn, Germany
[2]Institute of Astronomy of Kharkiv National University, Sumska Str. 35, 61022 Kharkiv, Ukraine
*Corresponding author: yevgen.grynko@upb.de

Received 30 March 2018; revised 14 June 2018; accepted 16 June 2018; posted 27 June 2018 (Doc. ID 327331); published 19 July 2018

We study the dependence of the intensity and linear polarization of light scattered by isolated particles with the compact irregular shape on their size using the discontinuous Galerkin time domain numerical method. The size parameter of particles varies in the range of $X = 10$ to 150, and the complex refractive index is $m = 1.5 + 0i$. Our results show that the backscattering negative polarization branch weakens monotonously, but does not disappear at large sizes, up to the geometrical optics regime, and can be simulated without accounting for wave effects. The intensity backscattering surge becomes narrower with increasing particle size. For $X = 150$, the surge width is several degrees.

OCIS codes: (290.0290) Scattering; (290.5850) Scattering, particles; (080.0080) Geometric optics.

https://doi.org/10.1364/OL.43.003562

The principal aim of the photometric and polarimetric remote sensing of the earth and solar system objects is to retrieve information about the properties of mineral grains that act as the solar light scatterers. Such particles have random morphologies, and their sizes vary from sub-micron scales to hundreds of microns. Solar light scattered at large scattering angles, close to the direction of backscattering, by isolated particles and powder-like surfaces (planetary regoliths), often exhibits the opposition phenomena: intensity surge (IS), i.e., nonlinear enhancement of intensity and negative polarization (NP) [e.g., 1–3], which can be related to each other.

Although the NP of ensembles of isolated randomly oriented particles of irregular shapes larger than or comparable to the wavelength was expected for long time [e.g., 4], this effect was reliably measured only recently [5–8]. As for the IS effect, this was studied in laboratories only partially, because of the restriction of the maximal scattering angle for available equipment. The single-particle effects of the IS and NP may significantly contribute to the analog effects for a powdered surface consisting of such particles [9,10]. For powdered surfaces, additional IS and NP mechanisms have been proposed based on the shadowing effect [11] and the coherent enhancement of backscattering [4,12–16]. Both of these effects are collective, and we do not consider them here, focusing on the single-particle scattering.

The parameters of the IS and NP strongly depend on the physical properties of the scatterers, which can be utilized in the data retrieval. However, the specific mechanisms of the backscattering phenomena are not very well explained so far. Light scattering calculations using the T-matrix method or its modifications [e.g., Ref. 17] do not suggest any clear explanation of these effects. The discrete dipole approximation method provides more possibilities for interpretation [18–20]. For instance, we may suppose that the opposition phenomena of discrete structures arise due to the interference of all possible trajectories that connect dipoles. This includes the direct and time reversal trajectories, the interference of which can produce both the IS and NP. The role of the field interaction with the vacuum/material interface of particles in the origin of the IS and NP produced by isolated particles also remains not fully clear. The behavior of the IS and NP at large size parameters $X = \pi d/\lambda$, where d is the largest particle dimension and λ is the wavelength, in the transition region between the wave and geometric optics regimes, at $X > 60$, also is not well known.

For further consideration, the problem of light scattering by particles with complex shapes and structures can be solved numerically with methods that allow arbitrary representations of shape geometries of particles. We note that for the solution of the problem, realistic model geometries should be taken, whereas perfect shapes such as spheroids or cubes cannot be representative due to their peculiar geometric properties. The computational complexity of the scattering problem grows quickly with the size of the model particles. If they are much larger than the wavelength, the problem may become multiscale, taking into consideration the particle surface roughness. The requirement of fine spatial discretization results in large computational meshes with millions of cells. High-performance computing (HPC) and appropriate numerical methods that allow parallelization become important.

In this Letter, we apply the discontinuous Galerkin time domain (DGTD) numerical method [21]. We use models of faceted particles of randomly irregular shapes to study the changes in scattering angle functions of the intensity and linear polarization of scattered light over a wide range of size parameters,

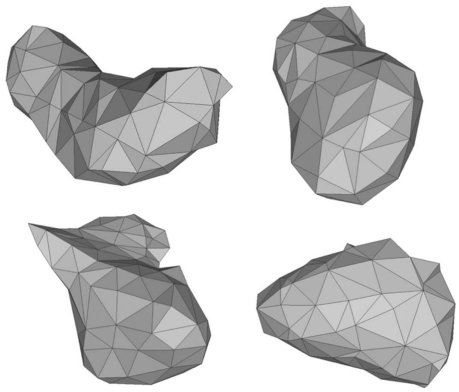

Fig. 1. Samples of GRF particles.

from the wavelength scale with $X = 10$ to the nearly GO regime of $X = 150$.

We use Gaussian random field (GRF) particles (Fig. 1) [22–24]. They mimic irregular shapes of compact mineral grains that can be found in many natural samples, in particular, in the lunar regolith [25]. We represent the geometries with sets of facets, which are convenient for insertion in the computational domain and an automatic tetrahedral unstructured mesh generation.

The propagation of the quasi-monochromatic plane wave in the computational domain is simulated by means of the total field/scattered field technique. In the scattered field region, the field components are Fourier-transformed then and a near-to-far-field transformation is applied to obtain the Jones matrix elements. Consequently, a 4×4 Mueller matrix F_{ij} is calculated for a range of scattering angles from 0° to 180°. Here we present only the intensity and linear polarization results, i.e., the element F_{11} and the ratio $-F_{21}/F_{11}$. For all size parameters, the scattering angle curves are averaged over the same set of 200 particle samples with each sample over six orientations. Additional averaging over 180 azimuthal scattering planes is also carried out in each simulation.

A numerical simulation of the electromagnetic scattering by particles much larger than the wavelength, i.e., with size parameters $X > 30$ requires large computational resources. We implemented a highly parallelized code and use the HPC facilities of the Paderborn University and JURECA of the Juelich Research Center. In the most complex case of $X = 150$, we operate with meshes with $\sim 10^7$ tetrahedral elements and requiring up to 100 24-CPU nodes on the JURECA cluster.

We also consider an extreme case of very large particles and apply a Monte Carlo GO model which is based on ray tracing in faceted particles and controlled by Fresnel's formulas and Snell's law [22–24].

In Fig. 2, we present the results of the DGTD calculations. One can distinguish three main features in the linear polarization curves [Fig. 2(a)]: the NP feature at scattering angles <120°, which is manifested especially for rather small particles; the positive polarization maximum; and the NP branch near backscattering. For the first time, to the best of our knowledge, we can compare such curves calculated with a numerically accurate method in the size range from small scale to the scale that is much larger than the wavelength. Interestingly, all main linear polarization features are preserved in the entire size range, including the NP feature at backscattering that becomes very small, but does not disappear [Fig. 2(b)]. We note the increasing role of the wave effects for the amplitude and the inversion angles where the polarization degree changes its sign.

Figure 2(c) shows the intensity dependencies of light scattered near the backscattering direction. One can see that single isolated particles are able to produce significant enhancement that resembles the intensity opposition effect observed for powder-like surfaces, including planetary regoliths. The degree of the IS enhancement correlates with the changing strength of the NP feature as the size parameter increases. As one may see, the IS becomes narrower with increasing particle size. For rather large particles, this result perhaps can be applied for interpretation of the opposition spike of the Saturn rings [26–28].

The size parameter of $X = 150$ corresponds to the scale of 48 wavelengths. This is close to the geometrical optics (GO) regime. In Fig. 3, we compare the DGTD data at $X = 150$ with the GO results calculated for the same set of samples. Considering the same number of orientations, we obtain a spiky curve that is a result of ray tracing on a limited number of facets. Therefore, we did calculations also for a larger number of orientations sufficient for smoothing the numerical noise. Both of these GO curves appear to be close to each other.

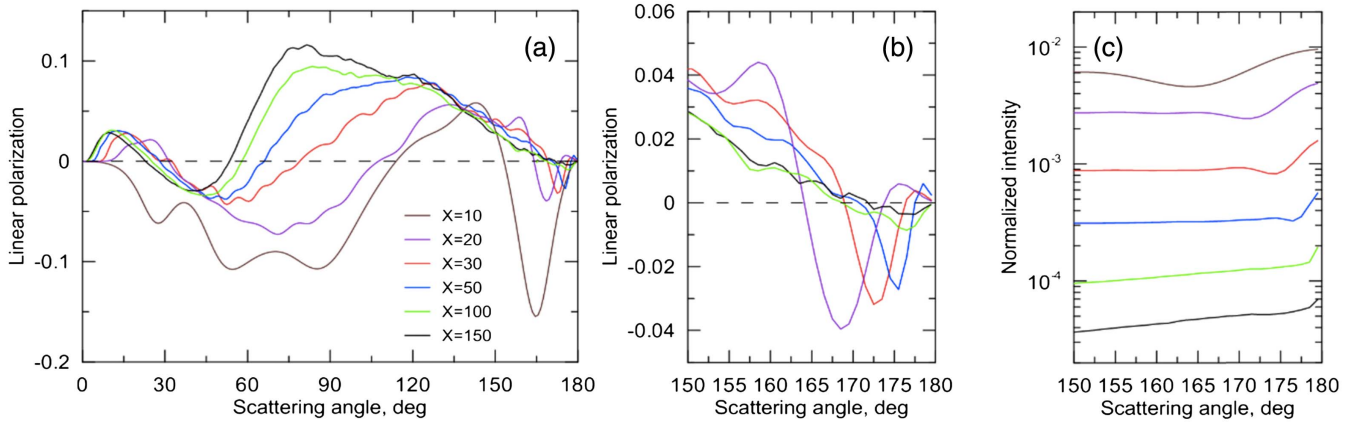

Fig. 2. Linear polarization versus scattering angle calculated with the DGTD method for six sets of GRF particles with different size parameters from $X = 10$ to 150 and complex refractive index $m = 1.5 + 0i$. Plot (a) shows the full range of scattering angles; (b) and (c), respectively, show the polarization degree and intensity dependencies near backscattering for the same particles as in (a).

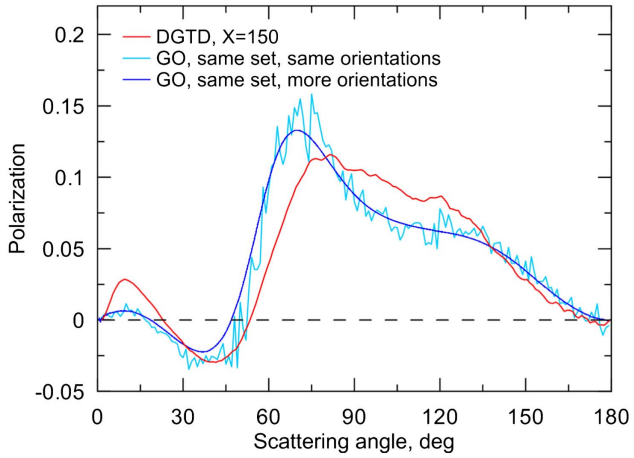

Fig. 3. Comparison of the linear polarization calculated with the GO model and the DGTD method with $X = 150$ and $m = 1.5 + 0i$. For the GO calculations, we used 10^9 rays.

There is also a decent agreement with the DGTD curve. For a better fit at all scattering angles, we would need the size parameter of at least $X = 200$ [29].

A comparison of the wave optics results with that obtained with the GO model allows us to extend the trajectory analysis to smaller size parameters. It becomes obvious that for smaller particles the polarization curves are formed by a similar mechanism, i.e., by the field interaction with the vacuum/material interface [22,30]. In Ref. [31], we showed that for $X = 50$ and highly absorbing smooth compact particles, the external scattering forms a polarization curve that follows simple Fresnel reflection functions with nearly 100% polarization near the Brewster angle. On the other hand, the result is different for the same size, if particles have agglomerated debris morphology [31].

In Fig. 4, we compare the IS calculated using the GO model and the DGTD method for $X = 150$. As we may conclude, the large particles can produce very narrow opposition spike of brightness, although the GO and DGTD trends are rather different. This spike effect is perhaps secondary for bright surfaces consisting of large transparent particles owing to a significant contribution of multiple scattering between particles.

We also note the IS near opposition in the case of pure GO (Fig. 4). This effect occurs since only at exact backscattering the direct, and all time-reversal trajectories come to the same angle bin. This produces an increased number of rays in other bins close to 180°, in comparison with other directions. This effect somewhat resembles the coherent backscatter enhancement, but without interference of rays. This IS has not been earlier noted in ray-tracing experiments, because it manifests itself only with a very large number of incident rays. The number should be enough to provide rays targeting the surface points for generation of the time reversal trajectories. We note that in natural and laboratory measurements the new geometrical backscattering effect and the coherent backscatter enhancement cannot be separated from each other. It should be emphasized that the described effect does not relate to the so-called retroreflection phenomenon [22,32,33].

Observing the decreasing depth and the inversion angle of the NP with the increasing size parameter, one could also expect that it is preserved in the extreme case of the GO regime. Previously, we also found that GO can produce the NP at backscattering in the special case of multiple scattering in dense media if the incidence angle is large enough to break the symmetry of illumination [34]. Here we again applied our GO model to a large ensemble of isolated particle samples and, surprisingly, found a very weak, but measurable, remnant of this feature.

Our GO analysis shows that the shape of the scattering angle curve is determined by the first few orders of scattering, i.e., the simplest ray trajectories: (1) external reflection, (2) transmission in the forward direction as a result of two refractions on the interface, (3) trajectories with one internal reflection, and (4) two internal reflections. Higher orders only suppress the sum of the first four, as they are almost totally depolarized [22–24]. In Fig. 5, we present the results of the GO calculations near backscattering well averaged over 10^5 irregular samples that also include concave shapes. Each point in the plot corresponds to the actual angular bin where the outgoing rays were collected. High-accuracy calculations with sufficient angular resolution demonstrate that the NP for randomly irregular

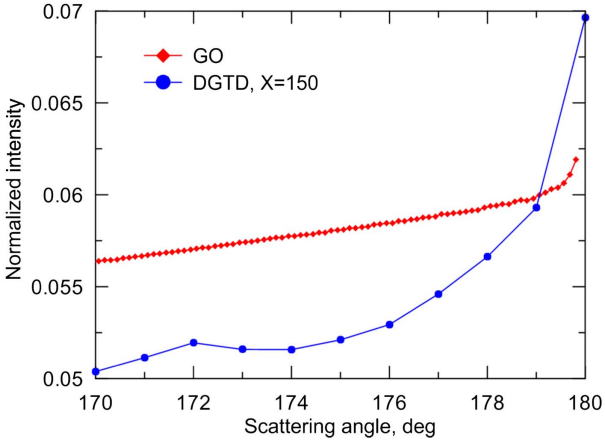

Fig. 4. Comparison of the IS calculated with the GO model and with the DGTD method for $X = 150$ and $m = 1.5 + 0i$. For the ray-tracing, we used 10^{12} rays.

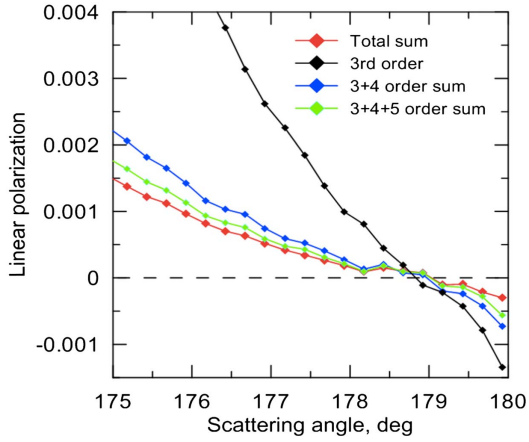

Fig. 5. Linear polarization near backscattering versus scattering angle calculated with the GO model and averaged over 10^5 samples; $m = 1.5 + 0i$. Each ratio $-F_{21}/F_{11}$ was calculated for the marked orders of scattering. For the ray-tracing we used 10^{12} rays.

particles can be formed, even in the GO approximation, and it becomes a persistent feature surviving averaging over many samples and orientations.

Considering the first few orders of scattering, one can see that the third and the fourth orders, i.e., the rays that experience one and two internal reflections are responsible for the formation of the NP. If these are total internal reflections then the rays are not depolarized between two refractions and, at some point, become similar to those that are simply transmitted in the forward direction. Two consequent refractions result in a strong NP [22–24] that we see at smaller scattering angles. The sum of these scattering orders gives an NP slightly smaller than 0.1%. Higher orders of scattering starting from the fifth (three internal reflections) depolarize the feature, and the total sum makes the NP weaker than 0.05%.

In conclusion, we note that with a parallel implementation of the DGTD method and HPC hardware, we are able to do systematic light scattering simulations for the size parameters up to $X = 150$. In the size range from $X = 10$ to 150 the polarization scattering angle curve does not change qualitatively. The backscattering NP feature is preserved up to the sizes where GO approximations become valid and can be obtained without accounting for wave effects.

Funding. Universität Paderborn.

Acknowledgment. The authors gratefully acknowledge the computing time granted by the Paderborn Center for Parallel Computing (PC^2) and by the John von Neumann Institute for Computing (NIC) on the supercomputer JURECA at Jülich Supercomputing Centre (JSC).

REFERENCES

1. B. Lyot, Ann. Obs. Meudon **8**, 1 (1929).
2. Y. Shkuratov, G. Videen, M. Kreslavsky, I. Belskaya, V. Kaydash, A. Ovcharenko, V. Omelchenko, N. Opanasenko, and E. Zubko, in *Remote Sensing*, G. Videen, Ya. Yatskiv, and M. Mishchenko, eds., NATO Science Series (Academic, 2004), pp. 191–208.
3. M. Mishchenko, V. Rosenbush, N. Kiselev, D. Lupishko, V. Tishkovets, V. Kaydash, I. Belskaya, Y. Efimov, and N. Shakhovskoy, *Polarimetric Remote Sensing of Solar System Objects* (Akademperiodyka, 2010).
4. Y. Shkuratov, K. Muinonen, E. Bowell, J. Peltoniemi, M. Kreslavsky, D. Stankevich, V. Tishkovetz, N. Opanasenko, and L. Melkumova, Earth Moon Planets **65**, 201 (1994).
5. O. Muñoz, H. Volten, J. de Haan, W. Vassen, and J. Hovenier, Astron. Astrophys. **360**, 777 (2000).
6. O. Muñoz, H. Volten, E. Rol, J. de Haan, W. Vassen, J. Hovenier, K. Muinonen, and T. Nousiainen, J. Geophys. Res. Atmos. **106**, 375 (2001).
7. O. Muñoz, H. Volten, J. F. de Haan, W. Vassen, and J. W. Hovenier, J. Geophys. Res. Atmos. **106**, 22833 (2001).
8. O. Muñoz, H. Volten, J. Hovenier, Y. Shkuratov, W. J. van der Zande, and L. B. F. M. Waters, Astron. Astrophys. **446**, 525 (2006).
9. Y. Shkuratov, A. Ovcharenko, E. Zubko, H. Volten, O. Muños, and G. Videen, J. Quant. Spectr. Rad. Trans. **88**, 267 (2004).
10. Y. Shkuratov, S. Bondarenko, V. Kaydash, G. Videen, O. Muñoz, and H. Volten, J. Quant. Spectr. Rad. Trans. **106**, 487 (2007).
11. B. Hapke, *Theory of Reflectance and Emittance Spectroscopy* (Cambridge University, 1993), p. 450.
12. Y. Shkuratov, Astron. Circ. **1400**, 3 (1985).
13. M. Mishchenko, J.-M. Luck, and T. Nieuwenhuizen, J. Opt. Soc. Am. A **17**, 888 (2000).
14. Y. Shkuratov, A. Ovcharenko, E. Zubko, O. Miloslavskaya, K. Muinonen, J. Piironen, R. Nelson, W. Smythe, V. Rosenbush, and P. Helfenstein, Icarus **159**, 396 (2002).
15. M. Mishchenko, J. Dlugach, L. Liu, V. Rosenbush, N. Kiselev, and Y. Shkuratov, Astrophys. J. Lett. **705**, L118 (2009).
16. R. M. Nelson, M. D. Boryta, B. W. Hapke, K. S. Manatt, Y. Shkuratov, V. Psarev, K. Vandervoort, D. Kroner, A. Nebedum, C. L. Vides, and J. Quinones, Icarus **302**, 483 (2018).
17. D. Petrov, Y. Shkuratov, and G. Videen, J. Quant. Spectrosc. Radiat. Transfer **113**, 2406 (2012).
18. E. Zubko, K. Muinonen, Y. Shkuratov, E. Hadamchik, A.-C. Levasseur-Regourd, and G. Videen, Astron. Astrophys. **544**, L8 (2012).
19. E. Zubko, G. Videen, and Y. Shkuratov, J. Quant. Spectrosc. Radiat. Transfer **151**, 38 (2015).
20. E. Zubko, Y. Shkuratov, and G. Videen, J. Quant. Spectrosc. Radiat. Transfer **150**, 42 (2015).
21. J. S. Hesthaven and T. Warburton, J. Comput. Phys. **181**, 186 (2002).
22. Y. Grynko and Y. Shkuratov, J. Quant. Spectrosc. Radiat. Transfer **78**, 319 (2003).
23. Y. Grynko and Y. Shkuratov, J. Quant. Spectrosc. Radiat. Transfer **106**, 56 (2007).
24. Y. Grynko and Y. Shkuratov, in *Light Scattering Reviews*, A. Kokhanovsky, ed. (Springer, 2008), Vol. **III**, pp. 329.
25. D. McKay, G. Heiken, A. Basu, and G. Blanford, in *Lunar Sourcebook*, G. H. Heiken, D. T. Vaniman, and B. M. French, eds. (Cambridge University, 1991), pp. 285.
26. F. A. Franklin and A. F. Cook, Astron. J. **70**, 704 (1965).
27. F. Poulet, J. N. Cuzzi, R. G. French, and L. Dones, Icarus **158**, 224 (2002).
28. R. M. Nelson, B. W. Hapke, R. H. Brown, L. J. Spilker, W. D. Smythe, L. Kamp, M. Boryta, F. Leader, D. L. Matson, S. Edgington, P. D. Nicholson, G. Filacchione, R. N. Clark, J.-P. Bibring, K. H. Baines, B. Buratti, G. Bellucci, F. Capaccioni, P. Cerroni, M. Combes, A. Coradini, D. P. Cruikshank, P. Drossart, V. Formisano, R. Jaumann, Y. Langevin, T. B. McCord, V. Mennella, B. Sicardy, and C. Sotin, *37th Annual Lunar And Planetary Science Conference* (2006).
29. Y. Grynko, Y. Shkuratov, and J. Foerstner, Opt. Lett. **41**, 3491 (2016).
30. Y. Grynko, Y. Shkuratov, and J. Foerstner, Opt. Lett. **38**, 5153 (2013).
31. Y. Grynko, E. Zubko, and J. Förstner, Opt. Lett. **39**, 6723 (2014).
32. T. S. Trowbridge, J. Opt. Soc. Am. A **1**, 1019 (1984).
33. K. Muinonen, K. Lumme, J. Peltoniemi, and W. M. Irvine, Appl. Opt. **28**, 3051 (1989).
34. Y. Grynko, Y. Shkuratov, and G. Videen, J. Quant. Spectrosc. Radiat. Transfer **101**, 522 (2006).